

## Research Papers

# Numerical and experimental investigation of a phase change material radial fin heat sink for electronics cooling

Mohammad Arqam<sup>a,\*</sup>, Laryssa Sueza Raffa<sup>a</sup>, Lee Clemon<sup>a</sup>, Mohammad Saidul Islam<sup>a</sup>,  
Matt Ryall<sup>b</sup>, Nick S. Bennett<sup>a</sup>

<sup>a</sup> School of Mechanical and Mechatronic Engineering, University of Technology Sydney, Ultimo, NSW 2007, Australia

<sup>b</sup> Mawson Rovers, Eveleigh, NSW 2015, Australia



## ARTICLE INFO

## Keywords:

Phase change material (PCM)  
Radial fin heat sink  
Thermal conductivity enhancer  
Thermal performance  
Electronic devices

## ABSTRACT

The recent advancements in miniaturization and multi-functionality of electronics have increased overheating risks, leading to unreliable performance and higher operating temperatures. To address this, a comprehensive numerical and experimental analysis of a 3D printed, stainless-steel, phase change material (PCM) radial fin heat sink design was performed. A three-dimensional unsteady numerical approach based on the finite volume method investigated the use of radial fins as thermal conductivity enhancers. A parametric study evaluated factors including power input, convective heat transfer coefficient, base thickness, fin thickness, and fin height. Paraffin wax was used as the PCM. To replicate the heat output of electronic devices, a constant power input was supplied to the heat sink base, capturing transient profiles of base temperature, volume average temperature, liquid-fraction, and velocity distributions. Results indicate that power input, convective heat transfer coefficient, and base thickness significantly influence performance more than fin thickness and height. Base temperature reductions with increased heat transfer, lower power input, and thicker bases were 81 %, 34.9 %, and 14.1 % respectively, while thicker and taller fins resulted in 4.3 % and 0.5 % reductions after 2000 s. The study suggests improved cooling performance with higher convective heat transfer coefficient ( $20 \text{ W/m}^2\text{K} < \text{HTC} < 40 \text{ W/m}^2\text{K}$ ), thicker bases ( $2 \text{ mm} < t_{\text{base}} < 3 \text{ mm}$ ), and thicker fins ( $1.5 \text{ mm} < t_{\text{fin}} < 2.5 \text{ mm}$ ) at constant power input. These findings contribute to the design and development of efficient heat sinks for high-power modern electronics.

## 1. Introduction

Efficient thermal management is of utmost importance in addressing the thermal issues associated with modern electronics. Ensuring the stabilization of temperatures at desired levels is imperative for performance, reliability, durability, and component safety. Given the electronics getting more compact with high power demand, the dissipation of excessive heat is a critical consideration to avoid potential operational failures. Nearly 50 % of failures observed in electronics can be attributed to elevated temperatures [1]. Conventional methods of active cooling reliant on forced convection have demonstrated the capacity to enhance the rate of heat transfer. However, these conventional cooling solutions, including components like fans and heat exchangers, present certain drawbacks such as bulky structure, increased weight, noisy operation, more power consumption, and the necessity for regular maintenance [2,3]. Consequently, such methods are often unsuitable.

In recent years, passive thermal management (PTM) of electronic

devices has incorporated the use of phase change materials (PCMs) in conjunction with numerous thermal conductivity enhancers (TCEs) viz. fins, metal foams, metal fibres and encapsulated PCMs [4–10] to improve their rate of heat transfer. This initiative is particularly crucial as PCMs, despite their effectiveness in latent heat absorption, demonstrate low thermal conductivity, which can result in poor heat dissipation. PCMs and TCE-based composite PTM systems have emerged as innovative solutions for passive cooling techniques across various domains such as personal computers, handheld devices, power electronics, high-performance lithium-ion batteries, and aerospace engineering [11–13]. The appeal of PCMs in electronics cooling lies in their properties, including a high latent heat of fusion at constant temperature [14].

Phase change materials can be categorized into three primary classes: organic, inorganic, and eutectic mixtures. These categories possess distinct thermophysical properties that underlie their diverse functionalities. Among these, organic PCMs, particularly those based on paraffin, are frequently preferred due to their broad range of melting

\* Corresponding author.

E-mail address: [Mohammad.Arqam@uts.edu.au](mailto:Mohammad.Arqam@uts.edu.au) (M. Arqam).

Nomenclature	
<i>FVM</i>	Finite volume method
<i>PCM</i>	Phase change material
<i>TCE</i>	Thermal conductivity enhancer
<i>TM</i>	Thermal Management
<i>HTC</i>	Heat transfer coefficient, W/m <sup>2</sup> K
<i>PTM</i>	Passive thermal management
<i>CAD</i>	Computer aided design
<i>EXP</i>	Experiment
<i>SIM</i>	Simulation
<i>ATM</i>	Atmosphere
<i>VAC</i>	Vacuum
<i>C</i>	Mush constant
<i>c<sub>p</sub></i>	Specific heat capacity, J/kgK
<i>ρ</i>	Density, kg/m <sup>3</sup>
<i>g</i>	Gravitational acceleration, m/s <sup>2</sup>
<i>H</i>	Height, mm
<i>k</i>	Thermal conductivity, W/mK
<i>L</i>	Latent heat of fusion, J/kgK
<i>m</i>	Mass, kg
<i>P</i>	Pressure, Pa
<i>u</i>	Velocity component in x direction, m/s
<i>v</i>	Velocity component in y direction, m/s
<i>w</i>	Velocity component in z direction, m/s
<i>S</i>	Source term in momentum equation
<i>3D</i>	Three dimensional
<i>W</i>	Width, mm
<i>t</i>	Time, s
<i>t<sub>fin</sub></i>	Fin thickness, mm
<i>t<sub>base</sub></i>	Base thickness, mm
<i>l<sub>fin</sub></i>	Fin height, mm
<i>T<sub>sol</sub></i>	PCM solid temperature, °C
<i>T<sub>liq</sub></i>	PCM liquid temperature, °C
<i>Q</i>	Power input, W
<i>Subscripts</i>	
<i>ini</i>	Initial
<i>l</i>	Liquid
<i>m</i>	Melting
<i>f</i>	Phase change material (liquid)
<i>ref</i>	Reference
<i>x, y, z</i>	Cartesian coordinates
<i>a, b, c</i>	Fitting coefficients
<i>Greek</i>	
<i>μ</i>	Viscosity, kg/ms
<i>β</i>	Thermal expansion coefficient, 1/K
<i>λ</i>	Liquid fraction
<i>δ</i>	Arbitrary small value

temperatures and high latent heat of fusion [15–17]. Choosing a suitable PCM depends on various factors such as thermal conductivity, specific heat capacity, latent heat of fusion, volume expansion during phase transition and low supercooling.

Phase change materials undergo a process of absorbing heat during phase transition from solid to liquid, and subsequently release this heat to the surrounding environment upon re-solidification [18,19]. The technique involving PCM/TCE for thermal management of electronics has three different stages. Initially, the PCM absorbs heat, inducing a gradual rise in PCM temperature towards the melting point, signifying the pre-sensible heating stage. Subsequently, the PCM achieves a roughly constant temperature at which melting commences, characterized by the absorption of latent heat while undergoing minimum volume expansion (<10 %) during the solid-to-liquid phase transition – an aspect encapsulated by the latent-heating phase. Lastly, the liquid PCM's temperature increases during post-sensible heating phase [20]. The use of PCMs spans numerous applications and domains, including air conditioning, aerospace, solar thermal technologies, water desalination, cooling of portable devices, and battery systems [21–27].

Numerous studies have investigated passive cooling techniques using a fin heat sink designs acting as TCEs impregnated with phase change materials. Researchers, such as Mahrous [28] have carried out experiments to evaluate the performance of PCM-based heat sinks. The study focused on determining the optimal setup and fin configuration. The findings revealed that the utilization of PCM reduces heating rates and consequently the peak temperature of heat sinks. Nayak et al. [29] conducted numerical simulations on three types of TCEs, namely porous matrix, plate-type fins, and rod-type fins, to enhance cooling capabilities. The results indicated that the performance of the heat sink is improved when the TCE material is distributed in thinner fins. Additionally, it was discovered that the rod-type fins outperform plate-type ones as they maintain better temperature uniformity within the PCM, resulting in lower chip temperatures. Similarly, in their study, Arshad et al. [30] conducted experiments on heat sinks with a specific shape referred to as round pins, utilizing paraffin wax. They evaluated the heat sinks with and without fins and concluded that a heat sink with a volumetric fraction of 1.0 (filled with PCM) demonstrated a greater

inclination to maintain the base temperature within lower, comfortable temperature limits compared to volumetric fractions of 0.0 and 0.5. Yazici et al. [31] conducted an experimental investigation to determine the combined effects of the number of fins and inclination angle on the cooling performance of a PCM heat sink with longitudinal plate fins. The study examined five heat sink geometries, varying in fin numbers from one to five under various inclination angles ranging from 0° (vertical) to 90° (horizontal), while maintaining a constant heating power of 16 W, both with and without PCM. The findings indicate a significant influence of both inclination angle and fin number on the development of convective cells within the liquid PCM domain, consequently affecting heat transfer and operating time. Moreover, the analysis indicates that the heat sink design featuring an inclination angle of 60° with three fins demonstrates better performance in terms of operating time. Meanwhile, Xie et al. [32] used numerical models to study how different fin shapes (plate and tree) influenced the heat sink's performance when exposed to natural convection.

Most numerical and experimental studies have focused on two types of fins i.e. plate and pin embedded with PCM [33–44]. For example, Shatikian et al. [37,38] used numerical models to see how changing the length, thickness, and space between fins affected the heat sink's temperature. They found that reducing the space between fins increased the melting rate. Likewise, Pakrouh et al. [39] developed numerical models to understand how changing the thickness and height of fins, along with the number of fins, impacted the heat sink's cooling performance. They concluded that the number of fins significantly reduced the heat sink's base temperature, followed by other parameters such as fin thickness, fin height, and base thickness. Moreover, Hosseinizadeh et al. [40] did experiments and numerical simulations on PCM embedded fin heat sinks to investigate how different parameters affected performance. They found that increasing the number of fins and their height, along with the power input, improved cooling, while changing the fin thickness had the least impact.

The literature review summary in Table 1 indicates that no prior studies have investigated the influence of radial fin geometry on the cooling performance of the heat sink. Therefore, this research aims to examine the potential advantages of using radial fins with paraffin wax

**Table 1**  
Studies published on phase change material fin heat sinks for electronics cooling.

Authors	Fin geometry	Analysis type	Boundary walls	Ambient	Application type
Mahrous [28]	Plate type	Experimental	Insulated, natural convection at the top	Atmosphere	Electronics cooling
Nayak et al. [29]	Matrix, plate, and rod type	Numerical	Insulated, natural convection at the top	Atmosphere	Electronics cooling
Arshad et al. [30]	Round pin type	Experimental	Insulated, natural convection at the top	Atmosphere	Electronics cooling
Yazici et al. [31]	Plate type	Experimental	Insulated	Atmosphere	Electronics cooling
Xie et al. [32]	Plate and tree type	Numerical	Insulated, adiabatic	Atmosphere	Electronics cooling
Ashraf et al. [33]	Circular and square pin type	Experimental	Insulated, adiabatic, natural convection at the top	Atmosphere	Electronics cooling
Kalbasi [34]	Plate type	Numerical	Insulated, natural convection at the top	Atmosphere	Electronics cooling
Fok et al. [35]	Plate type	Experimental	Insulated, natural convection at the top	Atmosphere	Electronics cooling
Wang et al. [36]	Plate type	Numerical	Insulated	Atmosphere	Electronics cooling
Shatikian et al. [37,38]	Plate type	Numerical	Insulated	Atmosphere	Electronics cooling
Pakrouh et al. [39]	Pin type	Numerical	Symmetry and adiabatic	Atmosphere	Electronics cooling
Hosseinizadeh et al. [40]	Plate type	Experimental/ Numerical	Symmetry/ adiabatic/pressure outlet	Atmosphere	Electronics cooling
Saha and Dutta [41]	Plate type	Numerical	Symmetry/adiabatic	Atmosphere	Electronics cooling
Yang et al. [42]	Plate type	Numerical	Natural/forced convection	Atmosphere	Electronics cooling
Abdi et al. [43]	Plate type	Numerical	Insulated	Atmosphere	Electronics cooling
Present study	Radial type	Numerical/ experimental	Convection in all directions	Atmosphere/ vacuum	Electronics cooling

in electronics cooling under both atmosphere and vacuum conditions. The novelty lies in designing a compact radial fin heat sink using additive manufacturing techniques and developing three-dimensional numerical models that consider phase change material as an energy-storing media and convection heat transfer to the surroundings in all directions. The research commences with numerical modelling followed by experimental validation, considering possible geometric enhancements to make the design compact while maintaining effective thermal performance. The ultimate aim is to provide insights for selecting the best fin geometry for efficient electronics cooling. This research contributes to decision-making in heat sink design and development for effective heat dissipation from high-power electronics. Additionally, future recommendations are provided to inform design engineers and researchers who wish to exploit the potential of phase change material radial fin heat sinks for better thermal performance of modern electronics.

## 2. Numerical model

### 2.1. Heat sink design

The heat sink, which is depicted in Fig. 1 (b), is made of stainless steel 316 L, and features internal radial fins that aid in heat dissipation from the base. It has overall dimensions of  $30 \times 30 \times 30$  mm and weighs 68 g. Additionally, it is equipped with four mounting lugs and two PCM injection holes at the top surface. The manufacturing process for the heat sink was through laser powder bed fusion. The machine used for printing was GE Concept Laser M2 Series 5 (400 W). The CAD model of the heat sink is shown in Fig. 1(a), a photograph of 3D prints in Fig. 1 (b) and the dimensions are displayed in Fig. 1 (c). A total of 14 cases (Case 1 being the base case) were analysed based on heat sink design configuration, power input, and convective heat transfer coefficients. The design of experiments for the parametric study is presented in Table 2 with the base case corresponding to the experimental conditions used for validation purpose.

#### 2.1.1. Figure-of-merits

The rationale for the proposed PCM-integrated radial fin heat sink lies in its dual functionality of thermal energy storage and dissipation. While it is true that enclosing the radial fins within a PCM-filled metal box reduces the surface area exposed to the surroundings, the PCM plays a critical role in absorbing and storing heat during peak loads, thereby preventing rapid temperature rises. The figure-of-merits for this system include its ability to maintain lower peak temperatures and delay temperature rise during transient thermal loads. This heat sink design is intended for applications where managing thermal peaks and ensuring long-term stability are more critical than immediate heat dissipation to the surroundings.

### 2.2. Numerical procedure

A 3D PCM-based radial fin heat sink model was developed using SolidWorks 2021, as depicted in Fig. 1. The performance of the heat sink was analysed by considering various parameters such as power input, convective heat transfer coefficient, base thickness, fin thickness, and fin height. ANSYS-Fluent 2021 R2, a commercially available computational fluid dynamics (CFD) package with a pressure-based finite volume method (FVM), was utilized to solve the governing equations. The PRESTO and PISO algorithms for pressure-velocity coupling were used in the simulation. The second order upwind scheme was applied to discretize the convective terms in the momentum and energy equations, while a first-order implicit scheme with a fixed time step was used for time discretization. The under-relaxation factors were set to 0.3, 0.7, 1, and 0.9 for pressure, velocity, energy, and liquid fraction, respectively. The residuals were set to  $10^{-4}$  for continuity and momentum and  $10^{-6}$  for energy equations. Physical dimensions of the model were obtained from the design and assumed that the material is uniform throughout. The flow of liquid PCM in the cavity was assumed to be laminar, Newtonian, and incompressible. The constant thermophysical properties of the stainless steel and PCM were assumed. The interface of melting was

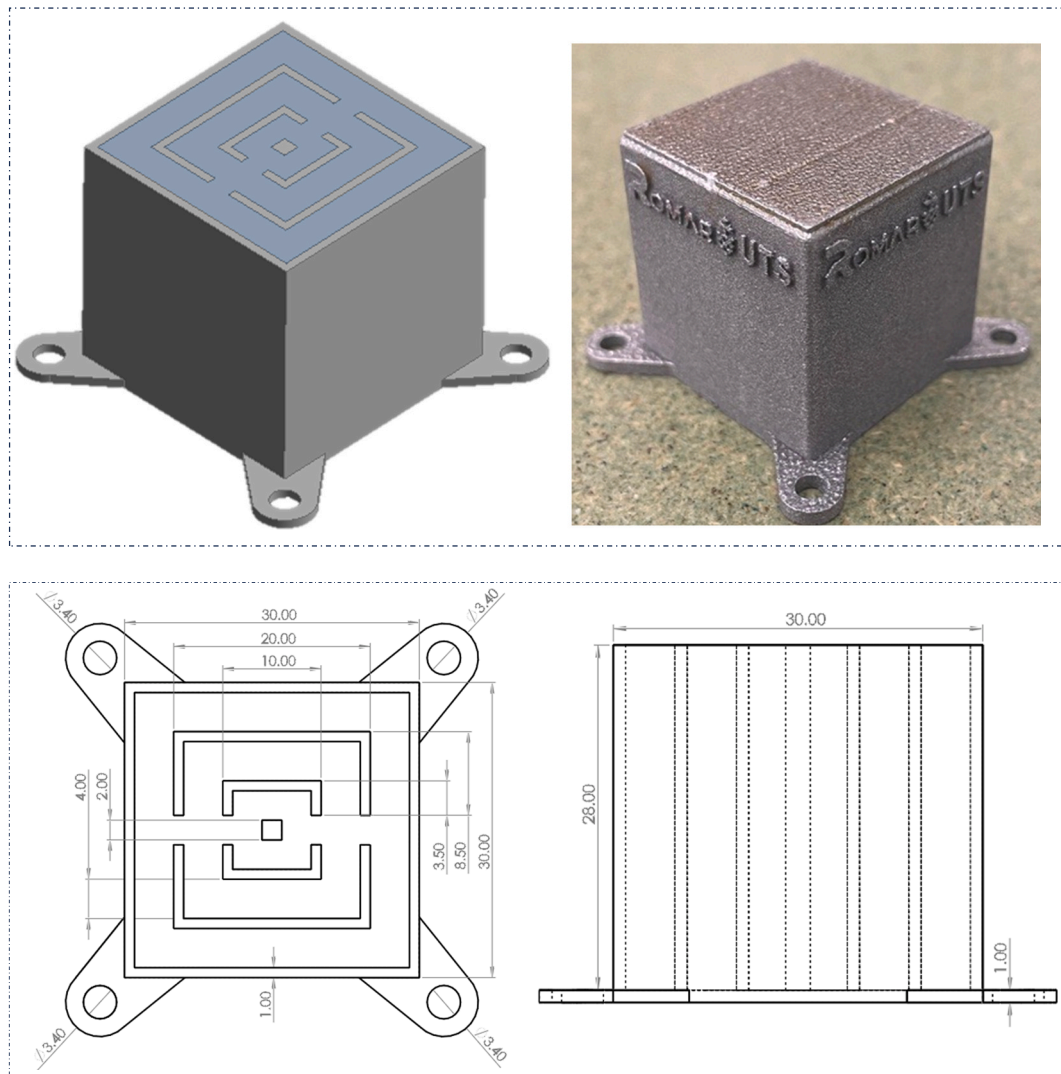


Fig. 1. Schematic diagram of heat sink (a) CAD model (b) 3D printed heat sink (c) heat sink dimensions – all in mm.

Table 2  
Design of experiments for parametric study.

Cases	Heat sink model			Power input (W)	HTC (W/m <sup>2</sup> K)	Description	Ambient
	$t_{base}$ (mm)	$t_{fin}$ (mm)	$l_{fin}$ (mm)				
1	1.0	1.0	28.0	9.0	40.0	With PCM	Atmosphere
2	1.0	1.0	28.0	8.0	40.0	With PCM	Atmosphere
3	1.0	1.0	28.0	7.0	40.0	With PCM	Atmosphere
4	1.0	1.0	28.0	6.0	40.0	With PCM	Atmosphere
5	1.0	1.0	28.0	9.0	30.0	With PCM	Atmosphere
6	1.0	1.0	28.0	9.0	20.0	With PCM	Atmosphere
7	1.0	1.0	28.0	9.0	10.0	With PCM	Atmosphere
8	2.0	1.0	28.0	9.0	40.0	With PCM	Atmosphere
9	3.0	1.0	28.0	9.0	40.0	With PCM	Atmosphere
10	1.0	1.5	28.0	9.0	40.0	With PCM	Atmosphere
11	1.0	2.0	28.0	9.0	40.0	With PCM	Atmosphere
12	1.0	1.0	23.0	9.0	40.0	With PCM	Atmosphere
13	1.0	1.0	18.0	9.0	40.0	With PCM	Atmosphere
14	1.0	1.0	13.0	9.0	40.0	With PCM	Atmosphere

characterized by the mushy zone, where the PCM is a mixture of solid and liquid phases. The Boussinesq approximation was implemented to account for the effects of buoyancy. The metal was assumed to remain in a solid state by absorbing only sensible heat. The volumetric expansion of the PCM during phase transition and heat transfer through thermal radiations were neglected [14,38,41]. Thermal resistance between the

heater chip and the base of the heat sink was also neglected. The necessary thermo-physical properties of the metal and PCM are listed in Table 3. Fig. 1 (c) includes 1 mm thick radial fins on the inside as a possible means for heat transfer enhancement.

**Table 3**  
Thermo-physical properties in the analysis.

Materials	Properties							
	Density ( $\frac{kg}{m^3}$ )	Specific heat ( $\frac{J}{kgK}$ )	Thermal conductivity ( $\frac{W}{mK}$ )	Viscosity ( $\frac{kg}{m.s}$ )	Thermal expansion coefficient, $\beta$ ( $\frac{1}{K}$ )	Latent heat, L ( $\frac{J}{kg}$ )	Solidus temperature ( $^{\circ}C$ )	Liquidus temperature ( $^{\circ}C$ )
Stainless Steel	8030	502.5	16.3	–	–	–	–	–
Paraffin Wax	880	2000	0.2	0.03	0.00011	170,000	53	58

### 2.3. Governing equations

The governing equations (continuity, momentum, and energy) for numerical analysis are as follows [14,29,42,43]:

$$\frac{\partial u}{\partial x} + \frac{\partial v}{\partial y} + \frac{\partial w}{\partial z} = 0 \quad (1)$$

$$\rho_f \left( \frac{\partial u}{\partial t} + u \frac{\partial u}{\partial x} + v \frac{\partial u}{\partial y} + w \frac{\partial u}{\partial z} \right) = -\frac{\partial p}{\partial x} + (\mu_f) \left( \frac{\partial^2 u}{\partial x^2} + \frac{\partial^2 u}{\partial y^2} + \frac{\partial^2 u}{\partial z^2} \right) - S_x \quad (2)$$

$$\rho_f \left( \frac{\partial v}{\partial t} + u \frac{\partial v}{\partial x} + v \frac{\partial v}{\partial y} + w \frac{\partial v}{\partial z} \right) = -\frac{\partial p}{\partial y} + (\mu_f) \left( \frac{\partial^2 v}{\partial x^2} + \frac{\partial^2 v}{\partial y^2} + \frac{\partial^2 v}{\partial z^2} \right) - S_y \quad (3)$$

$$\rho_f \left( \frac{\partial w}{\partial t} + u \frac{\partial w}{\partial x} + v \frac{\partial w}{\partial y} + w \frac{\partial w}{\partial z} \right) = -\frac{\partial p}{\partial z} + (\mu_f) \left( \frac{\partial^2 w}{\partial x^2} + \frac{\partial^2 w}{\partial y^2} + \frac{\partial^2 w}{\partial z^2} \right) + \rho_f g \beta (T_f - T_m) - S_z \quad (4)$$

where  $p$  is the pressure,  $\rho$  is the density, and  $\mu_f$  is the absolute viscosity.  $S$  is the source term expressed as:

$$S = \frac{C(1 - \lambda_l)^2}{\delta + \lambda_l^3} \quad (5)$$

The liquid fraction ( $\lambda_l$ ) varies from 0 to 1 (complete solid to complete liquid).  $C$  representing mushy zone parameter was set to the FLUENT default value of  $10^5$  [14]. The mushy zone parameter plays a significant role in modelling the phase change process and understanding its impact is crucial for accurate simulation results in the future work. The modified Carman-Kozeny equation (Eq. 5) is derived from the Darcy law that governs the flow in porous media. The standard Carman-Kozeny equation generally returns an infinite value for  $S$  at zero liquid fraction. To avoid division by zero, an arbitrary computational constant,  $\delta = 0.001$  is included in the modified equation [43].

Additionally, the energy equation for the PCM is as follows.

$$\rho_f C_{p,f} \left( \frac{\partial T_f}{\partial t} + u \frac{\partial T_f}{\partial x} + v \frac{\partial T_f}{\partial y} + w \frac{\partial T_f}{\partial z} \right) = k_f \left( \frac{\partial^2 T_f}{\partial x^2} + \frac{\partial^2 T_f}{\partial y^2} + \frac{\partial^2 T_f}{\partial z^2} \right) - \rho_f L \frac{\partial \lambda_l}{\partial t} \quad (6)$$

Temperature dependent liquid fraction is updated according to Eq. 7.

$$\lambda_l = \begin{cases} 0 & T_f \leq T_{sol} \\ \frac{T_f - T_{sol}}{T_{liq} - T_{sol}} & T_{sol} \leq T_f \leq T_{liq} \\ 1 & T_f \geq T_{liq} \end{cases} \quad (7)$$

And  $C_{p,f}$  is the specific heat and  $k_f$  is the thermal conductivity of the PCM.

For the solid material, the energy equation reduces to unsteady heat conduction.

$$\rho_s C_{p,s} \left( \frac{\partial T_s}{\partial t} \right) = k_s \left( \frac{\partial^2 T_s}{\partial x^2} + \frac{\partial^2 T_s}{\partial y^2} + \frac{\partial^2 T_s}{\partial z^2} \right) \quad (8)$$

where  $\rho_s$  is the solid density,  $C_{p,s}$  is the specific heat of the solid, and  $k_s$  is

the thermal conductivity of the solid.

### 2.4. Initial and boundary conditions

The initial and boundary conditions for the simulation are shown in Fig. 2. The outside walls and top surface of the heat sink were set to convection boundary conditions with a heat transfer coefficient (HTC) that has been modified to mimic the actual room and vacuum conditions. A uniform heat flux boundary was applied to the base of the heat sink to account for the heat dissipated from the heater chip. The heat rejected from the PCB heater was measured to be approximately 9.0 W divided by the bottom wall surface area, which was taken to be the magnitude of the uniform heat flux applied to the base. The initial temperature for all the simulations was  $23^{\circ}C$  and the initial velocity was assumed to be zero for all cases considered.

### 2.5. Grid sensitivity and independence analysis

An example of the mesh used for the calculation is shown in Fig. 2 (b). Fillets, rounded corners and the top lid were removed from the drawing prior to meshing to reduce the mesh size. A tetra/hexa mesh was converted into polyhedral to reduce the cell count and ensure the accuracy of the simulation. The mesh quality check was performed before initializing the solution, and only 1 % of the cells out of 718 K were found to be below 0.8 orthogonal quality. A grid sensitivity and independence analysis was conducted as one of the prerequisites of the CFD simulation. Five different grid sizes (0.35 to 0.7 mm) were considered to determine their effect on the simulation accuracy, as shown in Fig. 3. The maximum variation in melting time and average temperature was noted to be 0.8 % and 0.09 %, respectively as presented in Table 4. Grid 3 was deemed fit for all the simulations to obtain reasonable results with less computational time. Time step sensitivity analysis was performed through considering three different time steps: 1, 0.1 and 0.01 s. The maximum difference in temperatures and liquid fraction observed between time steps at equal physical times was <1 %, hence a time step of 0.1 s was deemed suitable for the results presented here.

## 3. Experimental validation of numerical model

### 3.1. Experimental setup

The experiment involves attaching a heat sink to a printed circuit board (PCB) equipped with an electric heater and thermistor. The temperature at the base of the heat sink is measured by the thermistor at 5-s intervals throughout the entire heating process to evaluate its performance in heat dissipation and storage. The thermistor is located at the centre of the heated area of the PCB (Fig. 4 (a)). The heat sink absorbs heat from the heater and transfers it to the PCM for storage. The temperature data from the thermistor is collected and processed by a BeagleBone Black micro-processor, which then transmits it to a web-based control dashboard wirelessly. Both the PCB and micro-processor are battery-operated. Fig. 4 shows a schematic diagram and a picture of the experimental setup.

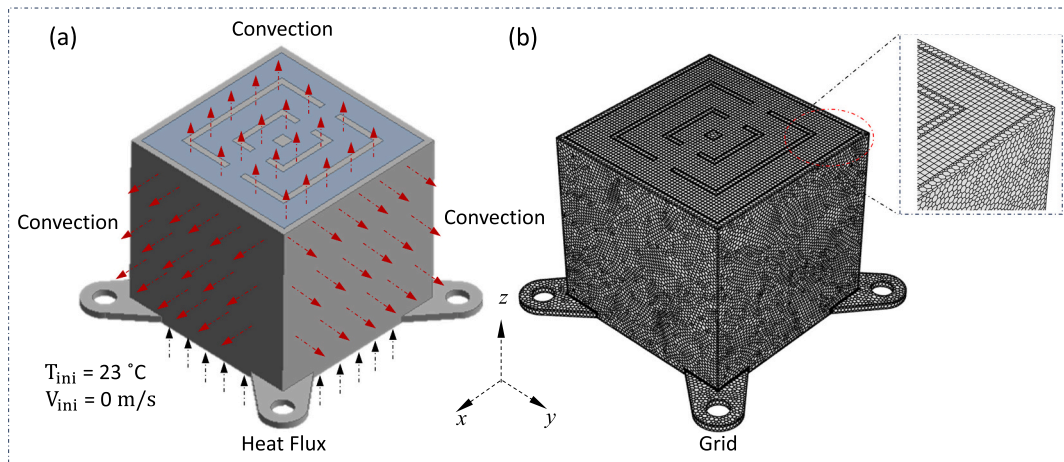


Fig. 2. (a) Initial and boundary conditions; (b) computational grid.

To evaluate the thermal characteristics of the heat sink devices, tests were conducted under different conditions, including with and without PCM, and testing under vacuum or at atmospheric pressure. For the tests performed with the heat sinks filled with PCM, an organic solid-liquid PCM was chosen due to its uniform melting properties, chemical stability, and relatively low change in volume during phase change. Based on the desired operating properties for the experiments, a paraffin wax with a melting point of 53 to 58 °C was adopted, i.e. Sigma-Aldrich 327,204 paraffin wax.

The custom-made PCB has a copper heater used as the thermal power source in the test setup. The heater heats up an area of  $30 \times 30 \text{ mm}^2$  at the centre of the PCB, where the heat sink is mounted. The resistance across the heater traces and the voltage of the PCB were measured using a digital multimeter, which showed values of  $3 \Omega$  and  $4.46 \text{ V}$ , respectively. According to Ohm's Law, these figures of resistance and voltage yield a thermal power input of  $9.0 \pm 0.5 \text{ W}$ . The multimeter's measurement uncertainty for resistance is  $\pm 1.5 \%$  and for voltage is  $\pm 0.5 \%$ . The NTCS0603E3103FMT thermistor, manufactured by Vishay, has a measurement uncertainty of  $\pm 1 \%$ .

### 3.2. Test procedure

Four variations of tests were performed as per Table 5.

To conduct the PCM tests, a liquid paraffin wax was injected into the heat sink via the PCM injection openings on the top surface. The PCM mass was 10 g, which, when in its liquid form, occupied a volume of 70 % of the available internal volume of the heat sink. The heat sink was mounted to the PCB using nylon nuts and screws to prevent heat dissipation through the screws via conduction. Note, the experiment was conducted with the heat sink oriented upside down, while the simulation considered an upright position, as the orientation effect is considered insignificant [45–47]. Additionally, a layer of Apiezon H thermal grease was applied between the heater and the bottom surface of the heat sink to minimize the thermal contact resistance. During the vacuum tests, a vacuum pump was used to maintain a pressure of 5 Pa in the chamber to reduce heat dissipation from the heat sink walls to the surroundings via convection. The chamber walls were made from polished metal to reduce heat exchange via radiation. The four variations of the experiment were conducted at room temperature, which was fixed at 22.5 °C. The initial temperature setpoint for the bottom surface of the heat sink was 23 °C with the heater turned off. Once the heater was switched on, the temperature at the heat sink's base was monitored and measured at 5-s intervals until it reached 100 °C. After the heater was shut off, the temperatures during cooldown were continuously monitored.

### 3.3. Comparison of simulation and experiment

Fig. 5 shows the experimental validation of the heat sink base temperature, both with and without PCM, at atmospheric conditions and in vacuum. As shown in Fig. 5 (a) and (b), there is a steady rise in temperature for the heat sink without PCM in both conditions. The base temperature reaches 100 °C in about 800 s in room conditions and 500 s in the vacuum chamber. The rapid temperature rise in the vacuum chamber can be attributed to the fact that there is minimal heat transfer through the heat sink walls to the outside, due to the limited heat transfer characteristics of the vacuum chamber. The use of a heat sink filled with PCM results in a low and stable temperature rise in both room and vacuum chamber conditions. The base temperature reaches 99 °C in 2000 s in room condition and 1200 s in vacuum. Additionally, the flattening of the curve is noted for the heat sink with PCM in both conditions, indicating that the melting of PCM is occurring within the heat sink. The difference between the two cases (with and without PCM) is due to the absence of latent heat storage. Once the melting is complete, the base temperature can rise to the same temperature as the heat sink without PCM. As a result, the continuous operation of the PCM-based heat sink is critical for its functionality, unless the application requires intermittent melting for the rejection of heat to the surrounding environment. The heat sink without PCM was simulated including air inside to allow maximum fin exposure to the surroundings. The results indicate that while both configurations (with and without PCM) perform similar initially, the design with PCM significantly outperforms in terms of maintaining lower base temperatures over extended periods, particularly during high thermal loads. The thermal resistance of the proposed PCM-integrated radial fin heat sinks was calculated and compared with the heat sink without PCM by measuring the temperature difference between the heat sink base and the ambient environment, divided by the power input. It was observed that the heat sink without PCM initially show lower thermal resistance, the PCM-integrated design maintains a more consistent thermal resistance over time due to the latent heat absorption properties of the PCM.

Another important point to consider is that the heat sink equipped with PCM can keep the base temperature at a lower level due to the fact that PCM has a much larger specific heat capacity (2000 J/kg. K) compared to air, which allows it to continuously absorb a significant amount of heat per unit kg at an increase of 1 K temperature when the base is heated. This is supported by the numerical simulation results, which agree well with the experimental results in the case of the heat sink with PCM (as shown in Fig. 5 (a) and (b)). However, the simulations do not account for the volume expansion of the PCM within the sink, resulting in a longer phase transition period and a larger amount of latent heat. Less PCM in the experiment leads to quick melting and the

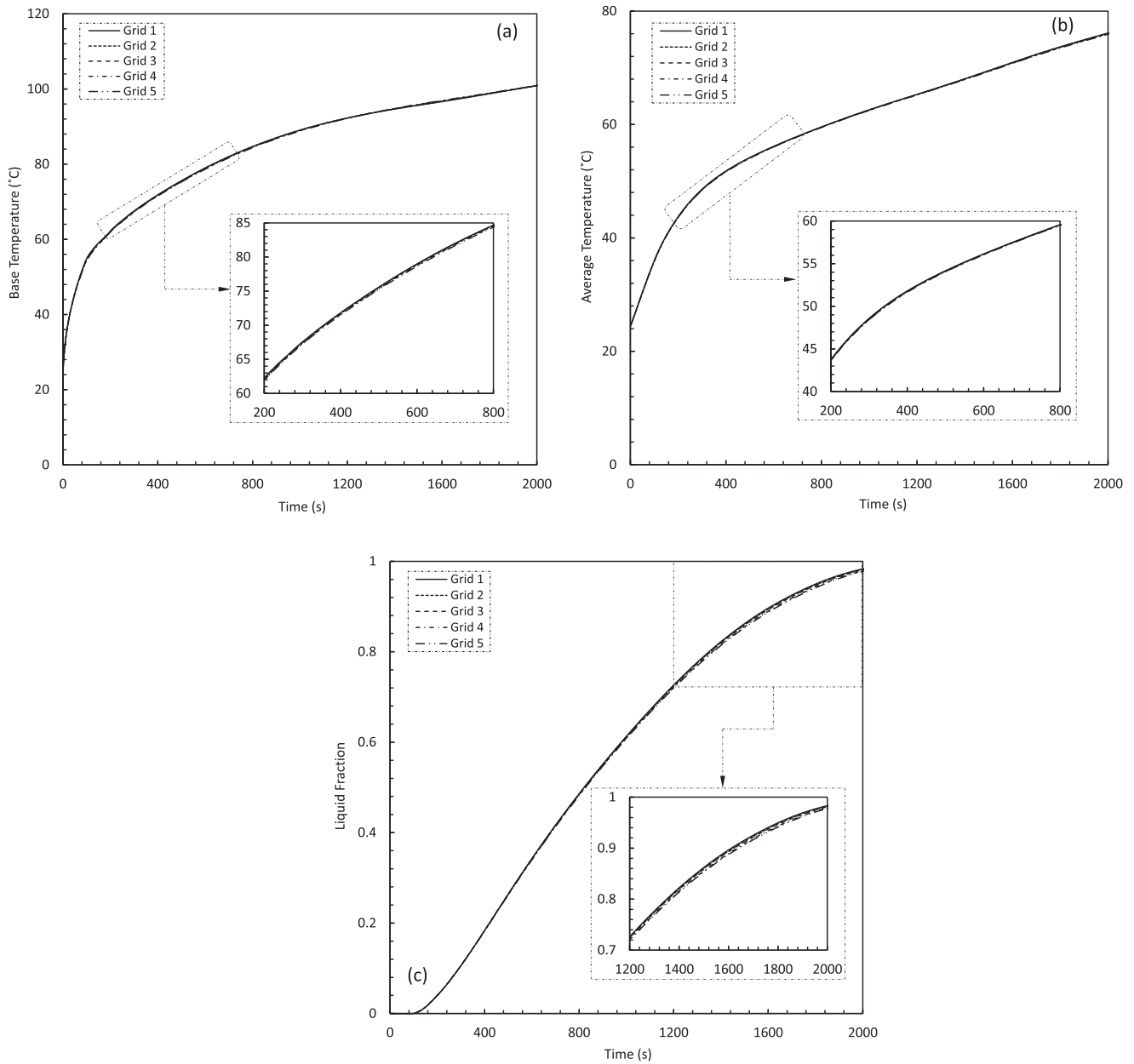


Fig. 3. Grid sensitivity analysis (a) base temperature; (b) average temperature; (c) liquid fraction.

**Table 4**  
Summary of grid sensitivity analysis.

Grid system	No. of cell	Melting time (s)	Deviation (%)	Avg. temp (°C)	Deviation (%)
Grid 1	281,818	2073	0.00	76.95	0.00
Grid 2	436,543	2085	0.58	77.01	0.08
Grid 3	718,503	2093	0.38	77.06	0.06
Grid 4	1,381,861	2110	0.81	77.13	0.09
Grid 5	2,035,042	2120	0.47	77.18	0.06

onset of the post-sensible heating phase. The difference in having more PCM and no volume expansion in the simulation is evident in the stability of the base temperature profiles since the heat exchange between the solid-liquid interface is through to the top and the unperturbed flow dynamics as seen in the liquid fraction evolution (Fig. 6), while in the experiment, the smooth heat transfer is only up to the middle of the cavity before the volume expansion occurs, which perturbs the flow

dynamics and hence the base temperature profiles. Additionally, the higher thermal conductivity of PCM (10 times) compared to air can explain the difference between the experiment and simulation results for the heat sink with PCM. In contrast, for the heat sink without PCM, the difference is primarily attributed to the disparity in thermal conductivity between the air region and the metal, which leads to numerical inaccuracies.

#### 4. Results and discussion

This section showcases the visualization of the liquid fraction, temperature, and velocity streamlines in the heat sink. It also highlights the impact of various parameters, such as power input, convective heat transfer coefficient, base thickness, fin thickness, and fin height on the system's performance.

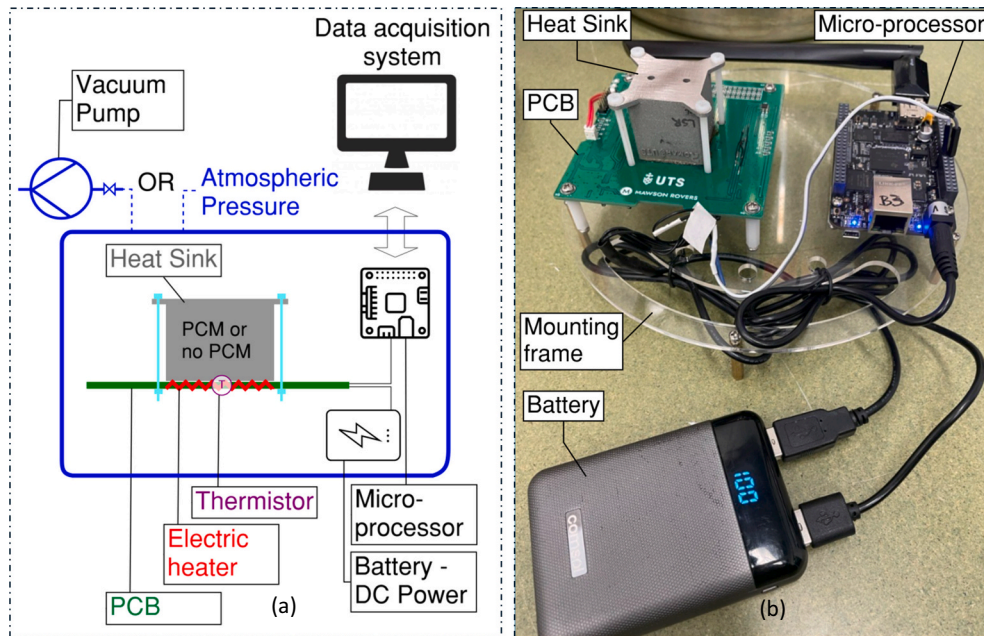


Fig. 4. Experimental set-up (a) schematic; (b) picture.

**Table 5**  
Variation of experimental tests.

Test variation	PCM mass (g)	Test conditions
1	0	Vacuum
2	10	Vacuum
3	0	Atmosphere
4	10	Atmosphere

#### 4.1. Evolution of liquid fraction

The inclusion of radial fins within the cavity, bottom wall heating, and convection heat transfer to the outside have a significant impact on the dynamics of molten PCM flow and the progression of the melt front, as depicted in Fig. 6. Initially, the PCM remains solid because all the heat supplied is used to increase the temperature of the metal until the system reaches the melting point of the PCM. Once the heat penetrates through the solid via conduction, melting begins at the metal-PCM interface and progresses towards the top, with more melting occurring along the fins/walls. To aid in visualization, liquid fraction, temperature, and velocity profiles are extracted only in the x-z and y-z planes as shown in Fig. 6 (a-c). The x-z plane displays the formation of Bernard convection cells due to bottom heating, which grow larger as melting progresses and move towards the top along with the natural convection flow initiated by the central fin. As melting nears completion, the onset of strong natural convection flow patterns near the fin suppresses the Bernard cells, resulting in a smoother flow pattern. A thermal stratification is formed as the solid PCM is melted at the top, and the formation of a wavy liquid fraction is partially due to the effect of buoyancy and wall heating when the hot PCM moves upward quickly near the wall/fin, and the liquid PCM adjacent to the solid chunk moves downward, resulting in a higher heat transfer rate near the fin and an inclined flow pattern. This phenomenon is supported by the literature presented in reference [43], where the authors explained the evolution of the liquid fraction inside the cavity with and without fins.

Radial fins within the cavity results in a smoother and unperturbed flow pattern, as evidenced by the y-z plane. The heat exchange at the fin-PCM interface generates a pair of counter-rotating convection cells that move along the fin length, promoting faster melting at the fins. The fin length accelerates the movement of these patterns and causes the PCM

between the fins to melt more rapidly. It is evident from Fig. 6 (a) and (c) that the convective flow near the fins has a stronger impact than the walls due to the external wall heat transfer to the surroundings in both planes. Fig. 6 (b) illustrates the transient temperature profiles for the heat sink during the physical melting time. As melting progresses, the heat sink's base and average temperature increase to 101 °C at 2000 s. Fig. 6 (c) and 7 show the velocity streamlines of the melted PCM inside the heat sink. As melting continues, the velocity of the molten PCM increases, reaching 0.65 mm/s upon complete melting. The streamlines in Fig. 7 depict the flow pattern of the molten PCM between the fins, with their corresponding velocities.

#### 4.2. Effect of power input

The impact of varying power input levels (6-9 W) on the performance of a heat sink with radial fins and PCM is illustrated in Fig. 8. The results show that as the power input increases, the melting process begins at an earlier time. Consequently, higher input levels result in higher base and average temperatures, which is expected because higher heating power led to a higher energy absorption rate by the PCM. There is a 10 °C difference in the base temperature between 8 W and 9 W at 2000s, while the difference decreases to 8 °C for power inputs of 6 W and 7 W. Additionally, the melt fraction with decreasing power input levels at 2000 s for 9 W, 8 W, 7 W and 6 W was found to be 98 %, 88 %, 71 %, and 51 %, respectively, as shown in Fig. 8 (c). The liquid fraction is proportionate with power input and can be calculated using a second order polynomial curve fitting expression found in Eq. 9. The purpose is to illustrate how the PCM transitions from solid to liquid phase as a function of the applied thermal load, thereby absorbing significant amounts of heat during the phase change process. This equation can help understand the thermal management capabilities of the PCM-integrated radial fin heat sink design presented here, as it directly relates to the amount of thermal energy that can be stored and subsequently dissipated during cooling periods. The black dot in Fig. 8 (a) contours represents the base temperature measurement's location corresponding to the temperature sensor location in the experiments. The maximum temperature and liquid fraction at 2000 s are provided in Table 6.

$$\lambda = aQ^2 + bQ - c \quad (9)$$

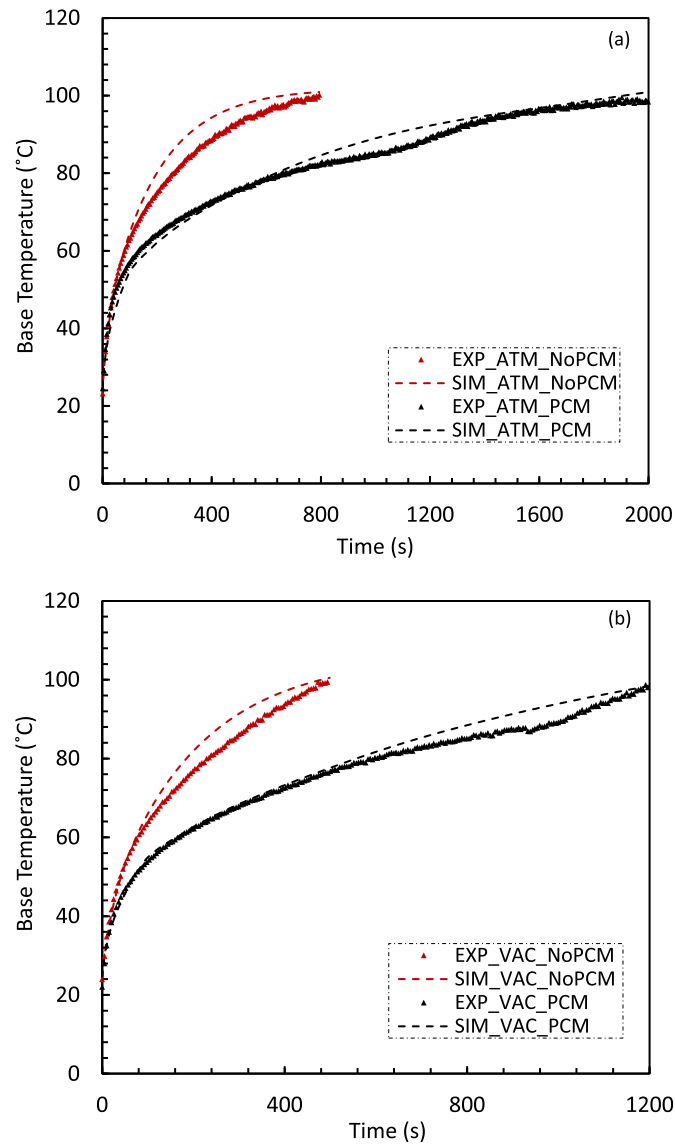


Fig. 5. Experimental validation (a) base temperature (atmosphere); (b) base temperature (vacuum).

where:

$$a = -0.025$$

$$b = 0.533$$

$$c = 1.79$$

$$R^2 = 0.994$$

#### 4.3. Effect of convective heat transfer coefficient

The effect of convective heat transfer coefficient ( $HTC = 10, 20, 30, 40 \text{ W/m}^2\text{K}$ ) on the overall thermal performance of the radial fin heat sink has been examined to address the cooling of high-power electronics working under natural and near-forced convection ambient conditions [42]. As shown in Fig. 9, the transient temperatures and liquid fraction profiles indicate that the effect of the convective heat transfer coefficient is significant. As shown in Fig. 9 (a), the heat sink base temperature is almost the same for all HTC values before the melting process begins, due to the main driving factor being the heating via conduction in the solid base. However, once the melting process starts, less heat transfer to

the ambient and the onset of natural convection between the solid-liquid interface inside the heat sink help to melt the PCM more quickly. At lower HTC values, more heat is absorbed at the base and transferred to the PCM, which results in an earlier melting process, while for higher HTC values, the heat sink releases more heat to the surrounding environment, which reduces the base and average temperature and increases the melting time for the PCM. It should be noted that after the complete melting of the PCM, the temperature rise is due to pure sensible heating caused by the power input supplied at the base. For a power input of 9 W and an HTC of  $40 \text{ W/m}^2\text{K}$ , 98 % of the PCM was melted in 2000 s, and the heat sink did not enter the post-sensible heating phase. The simulation time (2000 s) was selected to match the experiment run time. The maximum temperatures and liquid fraction at 2000 s are listed in Table 7.

#### 4.4. Effect of base thickness

The effect of base thickness on the thermal performance of the radial fin heat sink has been examined in Fig. 10. Three different thicknesses of the base i.e. 1, 2, and 3 mm, were considered to determine the performance in terms of base temperature, volume average temperature, and liquid fraction. As shown in Fig. 10, the temperatures and liquid fraction

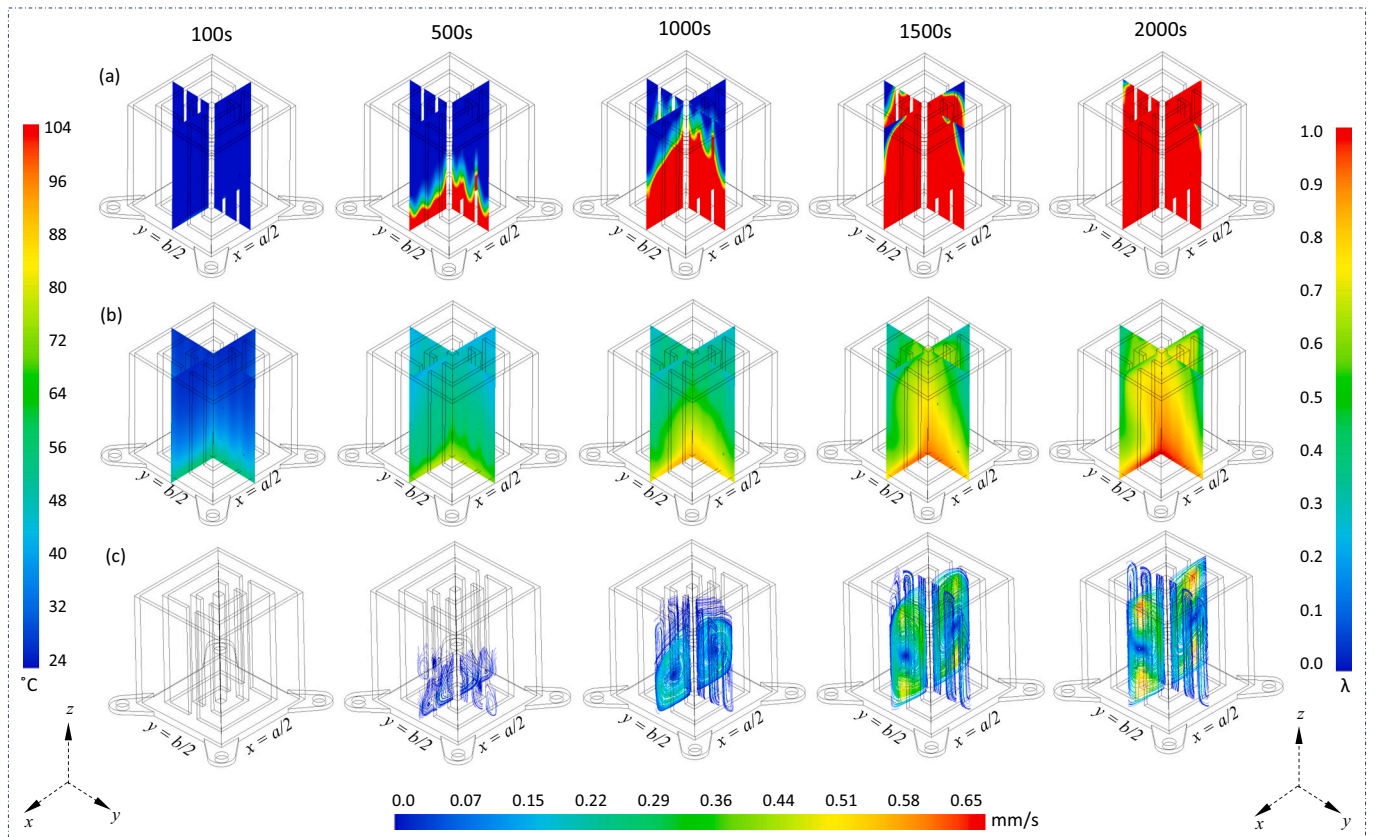


Fig. 6. Transient contours (a) liquid fraction; (b) volume average temperature; (c) velocity streamlines.

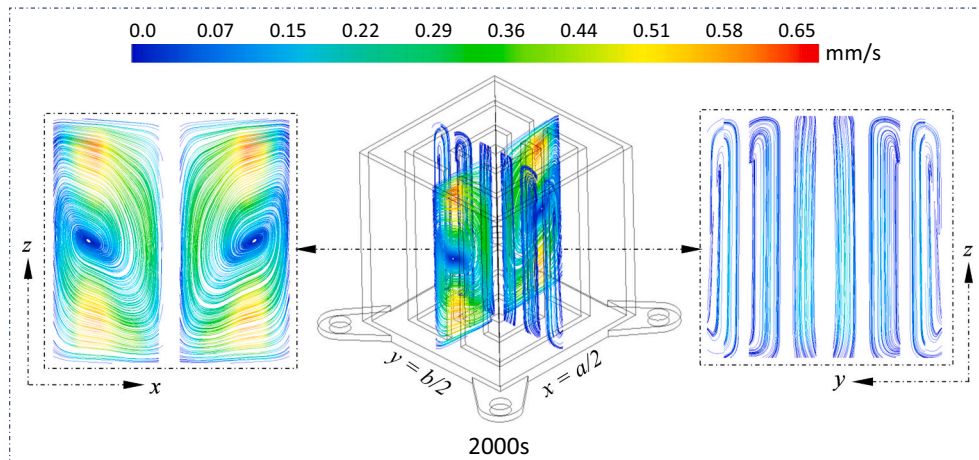


Fig. 7. Velocity streamlines at 2000s.

profiles indicate that the base thickness effect is less significant than the convective heat transfer coefficient. The thicker the base, the lower the base and average temperatures, and the slower the melting of the PCM. This is because more thermal mass leads to slower heat transfer. The difference in base temperature between 1 mm and 2 mm base is 7 °C, while the difference between 2 mm and 3 mm is only 5 °C at 2000 s. This suggests no significant difference between bases thicker than 3 mm. A thinner base would reduce the material needed for manufacturing, weight, and cost. However, the melting curve slope for all thicknesses is the same, as shown in Fig. 10 (c). Additionally, the slower melting observed with thicker base is due to the extra time it takes for heat to penetrate through the base via conduction. The temperature and liquid

fraction data at 2000 s is provided in Table 8. The red circles in the blown-up image in Fig. 10 (a) demonstrate a delay in PCM melt start corresponding to the base thickness. More thickness leads to a prolonged sensible heating phase since the dominating mode of heat transfer is conduction during this period.

#### 4.5. Effect of fin thickness

The influence of fin thickness on the thermal performance of the radial fin heat sink has been examined (as shown in Fig. 11), with three different thicknesses (1 mm, 1.5 mm, and 2 mm) being considered. The results show that the effect of fin thickness is relatively minor, with

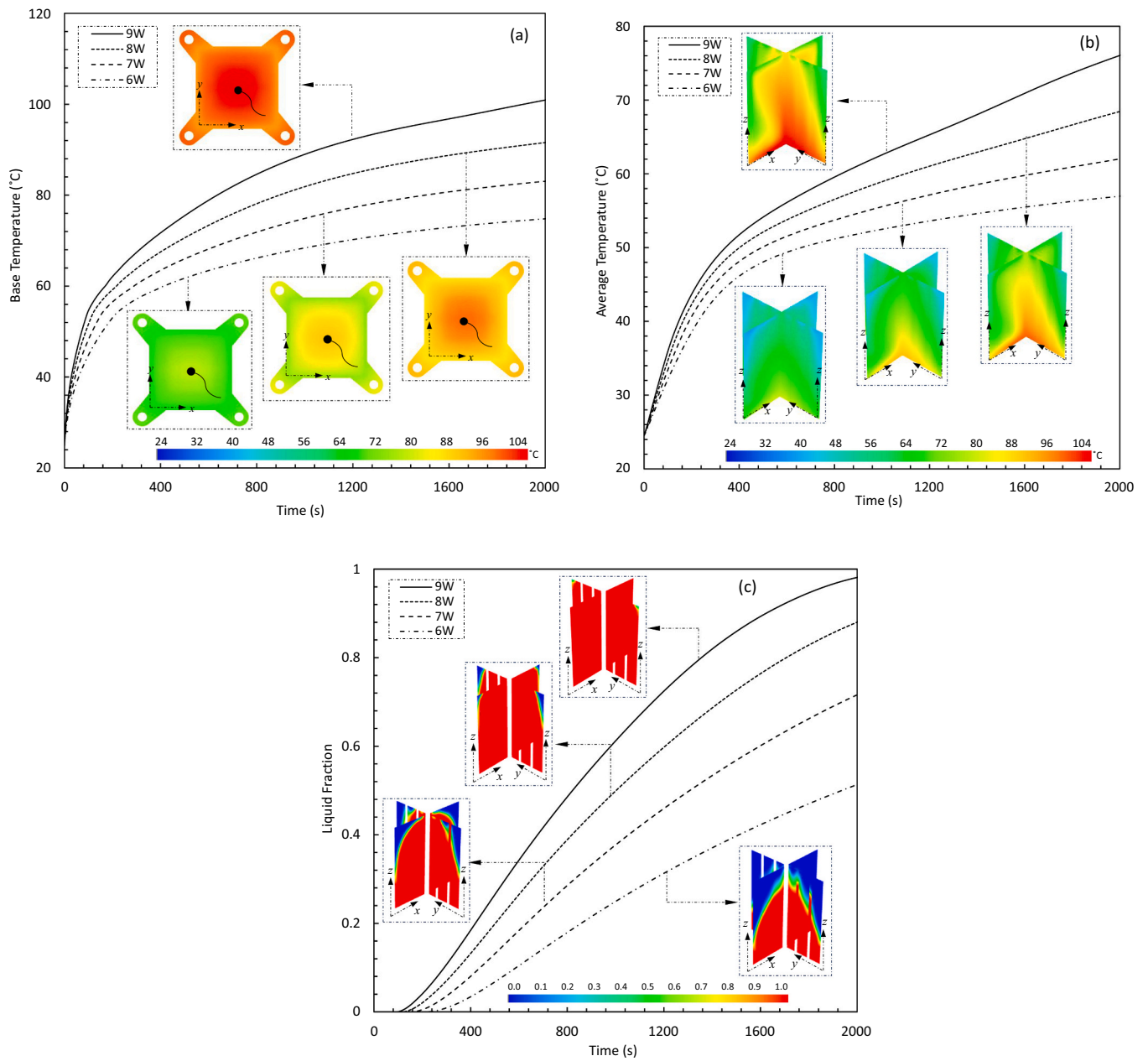


Fig. 8. Effect of power input (a) base temperature; (b) average temperature; (c) liquid fraction.

Table 6

Temperature and liquid fraction for cases (1, 2, 3, 4) at 2000 s.

Power input (W)	Base temp (°C)	Avg. temp (°C)	Liquid fraction (%)
6	74.8	57.0	51
7	83.1	62.0	71
8	91.5	68.4	88
9	100.9	76.1	98

thicker fins providing slightly better performance due to reduced thermal resistance. It should be noted that too thick fins may limit the functioning of PCM as a latent energy storage material by allowing only a small amount of PCM inside the cavity. The slight difference in base temperature in Fig. 11 (a) is due to more solid material and less PCM, which allows for faster heat transfer between solid and liquid interfaces via conduction and natural convection, while keeping a constant convective heat transfer coefficient for all cases. Fig. 11 (c) shows that

the melt start time of PCM in thicker fins is delayed due to conduction as the dominating mode of heat transfer. The temperature gradient required for conduction increases in proportion to the thickness of the fins, resulting in a higher heat transfer rate. As the fins become thinner, the temperature gradient increases, allowing for a higher rate of heat conduction and faster melting of the PCM. Conversely, thicker fins have a shorter melting time due to a lower amount of PCM, which results in a lower latent heat capacity. The temperature and liquid fraction profiles at 2000 s are provided in Table 9.

#### 4.6. Effect of fin height

The influence of fin height has been examined in Fig. 12. Four different fin heights, i.e. 13 mm, 18 mm, 23 mm, and 28 mm, were considered to investigate the effect of fin height on the base temperature, volume average temperature, and liquid fraction. The transient temperatures and liquid fraction profiles in Fig. 12 reveal that the fin

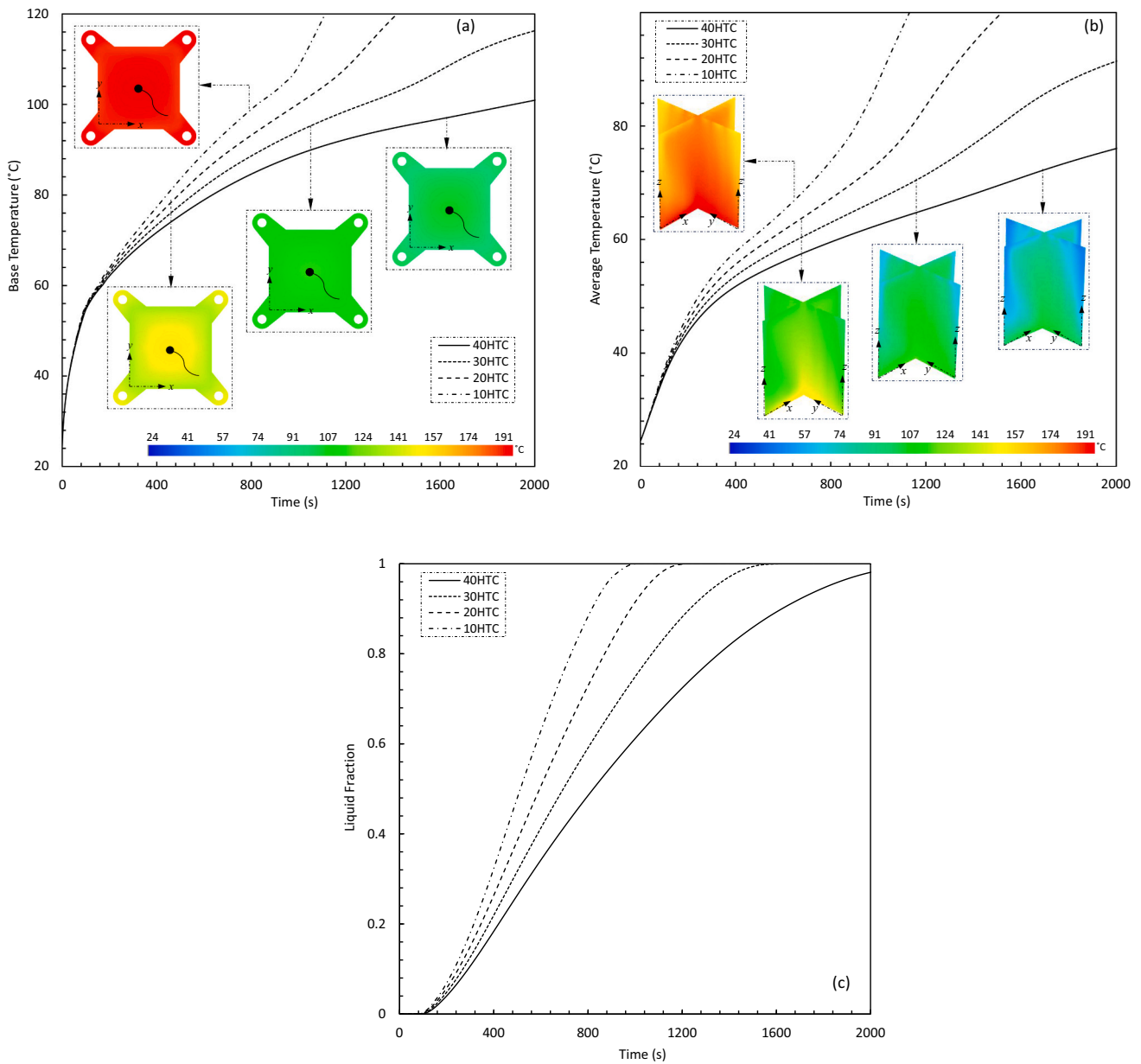


Fig. 9. Effect of convective heat transfer coefficient (a) base temperature; (b) average temperature; (c) liquid fraction.

**Table 7**  
Temperature and liquid fraction for cases (1, 5, 6, 7) at 2000 s.

HTC (W/m <sup>2</sup> K)	Base temp (°C)	Avg. temp (°C)	Liquid fraction (%)
10	183.1	158.2	100
20	139.7	114.7	100
30	116.3	91.4	100
40	100.9	76.0	98

height significantly influences the heat sink's performance particularly in stabilising the base temperature and more uniform melting of the PCM. As shown in Fig. 12, the heat sink's performance improves with increasing fin height. This is expected because the increased fin height enables more area for heat exchange between the solid-solid and solid-liquid interfaces. For smaller fins, the heat transfer starts from the base to the fins, and then the exchange happens only to a small amount of PCM in contact with the fins. The upper portion of the PCM (not in contact with fins) exhibits slow heat transfer because of the low thermal

conductivity of the PCM, which results in local overheating of the fins and base, thereby increasing the base temperature. Taller fins (28 mm) allow heat transfer between a larger portion of fins and PCM. Once the PCM near the walls and fins has melted, the onset of natural convection occurs, facilitating the rapid transfer of heat to the upper regions of the PCM. As depicted in Fig. 12 (c), the early commencement of the liquid fraction is attributed to the lower specific heat capacity of the shorter fins. For the same fin thickness, the lower specific heat capacity results in a more rapid rate of temperature increase for a given power input, enabling the heat sink to reach the melting temperature more quickly than the taller fins, and thus, initiating the PCM melting process earlier. A sharp slope of liquid fraction curve along the fin length in Fig. 12 (c) explain the effect of increased natural convection heat transfer rate on the melting process. As the solid-liquid interface moves past the fin tips, the melting rate decreases due to the contribution of Bernard circular cells. The temperature and liquid fraction profiles at 2000 s are provided in Table 10.

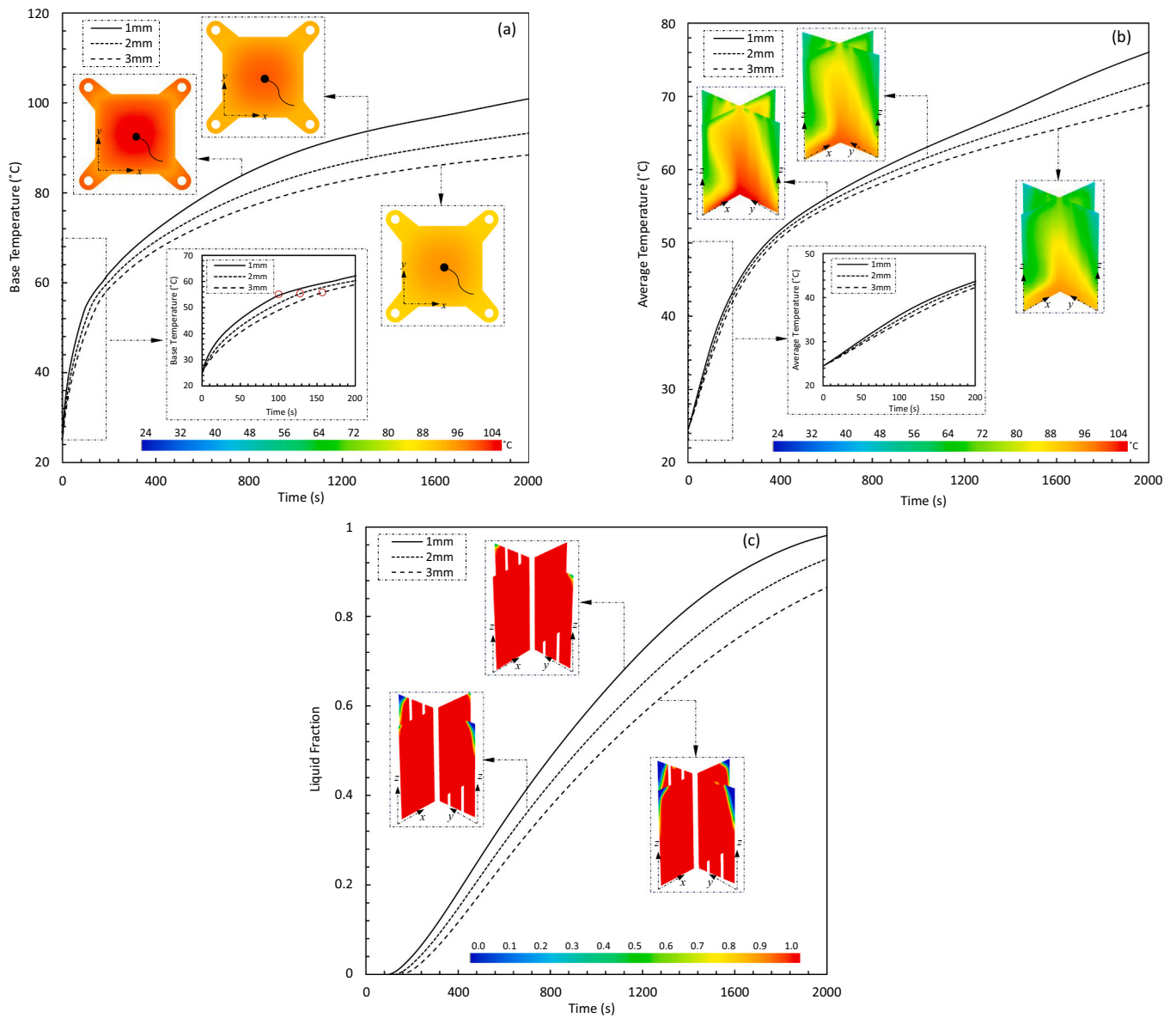


Fig. 10. Effect of base thickness (a) base temperature; (b) average temperature; (c) liquid fraction.

Table 8  
Temperature and liquid fraction for cases (1, 8, 9) at 2000 s.

Base thickness (mm)	Base temp (°C)	Avg. temp (°C)	Liquid fraction (%)
1.0	100.9	76.0	98
2.0	93.2	71.8	92
3.0	88.4	68.7	86

### 5. Conclusions and future recommendation

This research provides a comprehensive numerical and experimental analysis of a stainless-steel radial-fin heat sink with the aim of enhancing the thermal performance of modern electronics. The study examines the effectiveness of using radial fins as a TCE in conjunction with PCM. Additionally, a parametric study was conducted to investigate the influence of power input, convective heat transfer coefficient, base thickness, fin thickness, and fin height on the overall cooling performance. The results indicate that incorporating PCM into the radial-fin heat sink design leads to a lower base temperature and more uniform melting. Based on the findings, the following conclusions have been drawn:

- Reducing power input typically leads to a decline in temperature and an elongated melting time. For instance, at a power input of 6 W and duration of 2000s, only 50 % of the PCM melts, while at 9 W, 98 % of the PCM melts. The difference in base temperature between these two cases is 34.9 %.
- An increase in heat transfer to the ambient environment results in a more effective heat sink for storing latent heat over an extended period, rather than transitioning to the post-sensible heating phase sooner. In fact, the complete melting process takes twice as long when the heat transfer coefficient changes from 40 to 10 W/m<sup>2</sup>K. The difference in base temperature between these two cases is 81 %.
- The thickness of the base in the heat sink affects the heat transfer rate and the stability and temperature of the PCM. A thicker base lead to a slower heat transfer rate and a more stable, lower temperature. For example, there is a 14.14 % difference in base temperature between heat sinks with a 1 mm and 3 mm thick base.
- The fin thickness also plays a role in limiting the amount of PCM that can be embedded in the system, resulting in slower melting at the start and quicker at the end. Additionally, thinner fins result in a

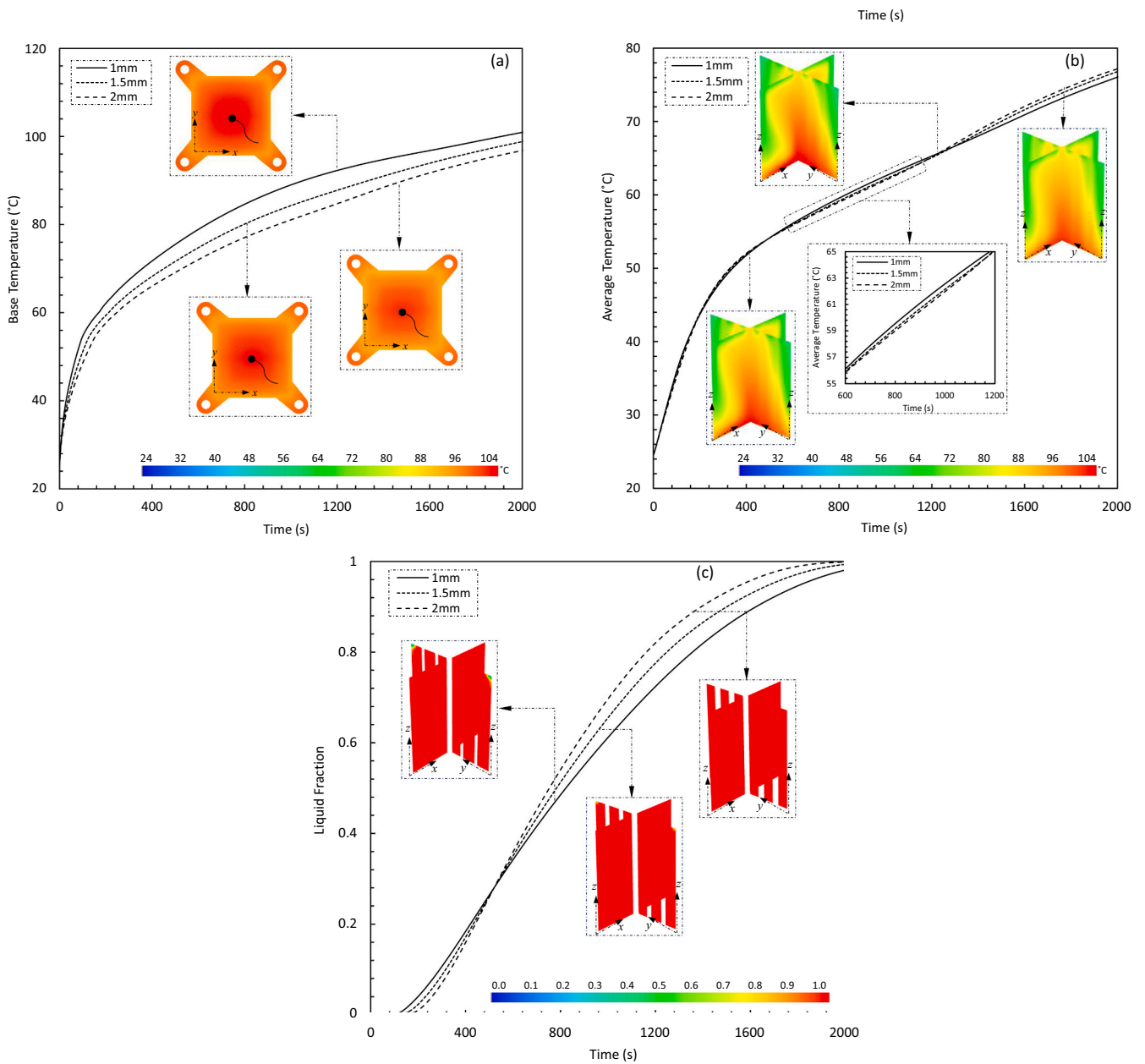


Fig. 11. Effect of fin thickness (a) base temperature; (b) average temperature; (c) liquid fraction.

Table 9

Temperature and liquid fraction for cases (1, 9, 10, 11) at 2000 s.

Fin thickness (mm)	Base temp (°C)	Avg. temp (°C)	Liquid fraction (%)
1.0	100.9	76.0	98.1
1.5	98.8	76.7	99.3
2.0	96.7	77.1	99.8

slightly higher base temperature at the end of the melting process, with a difference of 4.3 %.

- Fin height is a crucial factor in maintaining stability during the melting process. Shorter fins lead to more chaotic flow beyond the fin length, while taller fins with a cavity height result in a more stable and uniform flow.

The findings reveal that the influence of power input, convective heat transfer coefficient, and base thickness is more significant than fin

thickness and height. The study concludes that incorporating radial fins as TCE significantly enhances the heat transfer performance through stabilising base temperature and more uniform melting of PCM. The key contributions of this study include the novel insights into the performance of PCM-embedded radial fins under various conditions, the significant factors influencing heat sink performance, and the practical implications for the design and advancement of heat sinks for electronic cooling systems. It is recommended that future work focus on optimizing fin spacing with respect to height to identify the optimal heat sink geometry along with the effect of altering mushy zone parameter on the phase change process. The outcomes of this research will be valuable for design engineers and researchers who wish to utilize the potential of phase change material radial fin heat sinks to improve the thermal performance of modern electronics.

**CRedit authorship contribution statement**

Mohammad Arqam: Writing – review & editing, Writing – original

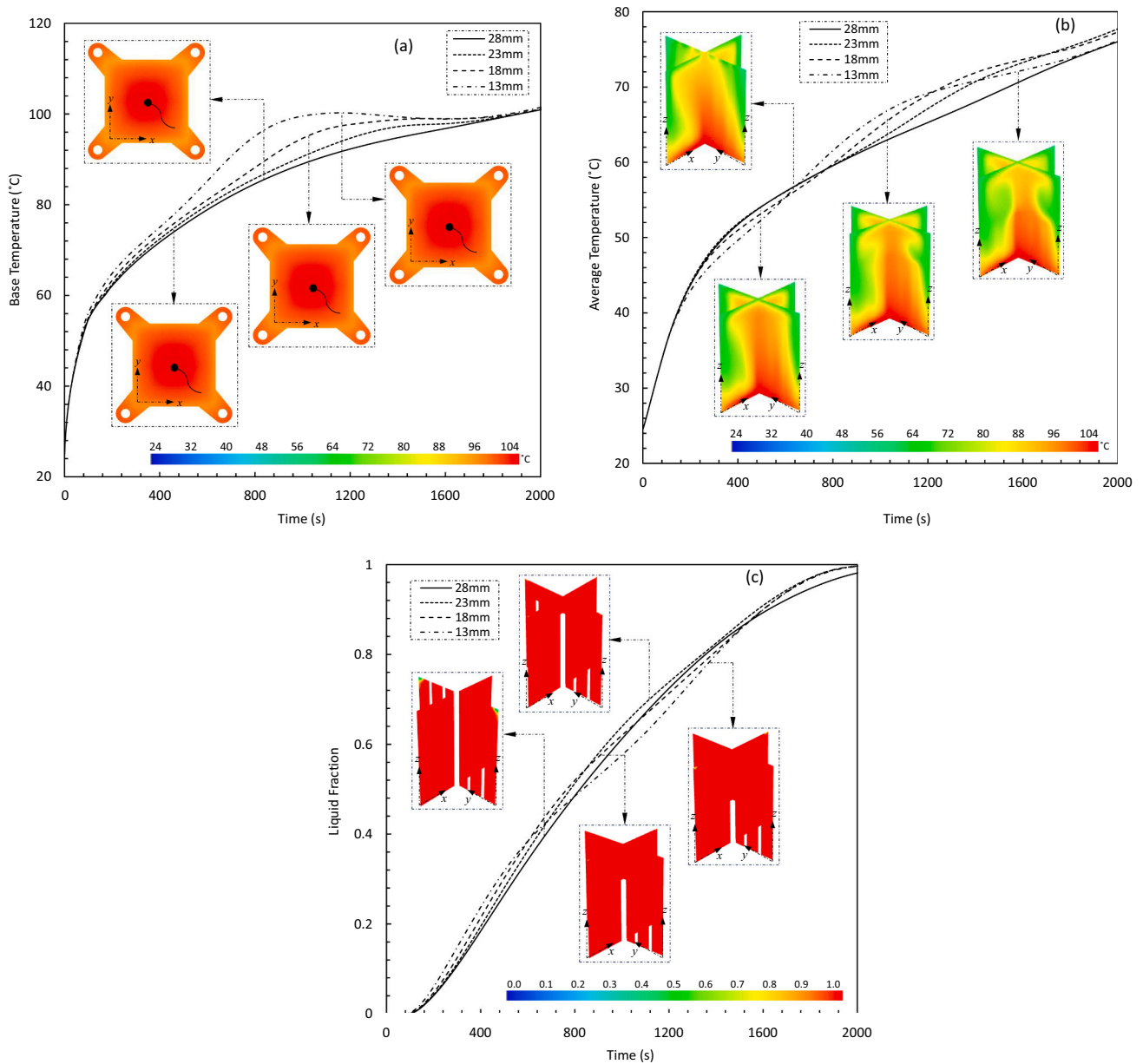


Fig. 12. Effect of fin height (a) base temperature; (b) average temperature; (c) liquid fraction.

**Table 10**  
Temperature and liquid fraction for cases (1, 12, 13, 14) at 2000 s.

Fin height (mm)	Base temp (°C)	Avg. temp (°C)	Liquid fraction (%)
13.0	101.4	76.1	99.5
18.0	101.1	77.3	99.6
23.0	101.0	77.7	99.6
28.0	100.9	76.0	98.1

draft, Visualization, Validation, Software, Methodology, Formal analysis, Conceptualization. **Laryssa Suezza Raffa:** Writing – review & editing, Writing – original draft, Validation, Data curation, Conceptualization. **Lee Clemon:** Writing – review & editing, Supervision, Resources, Project administration. **Mohammad Saidul Islam:** Writing – review & editing, Supervision, Funding acquisition. **Matt Ryall:** Writing – review & editing, Resources, Project administration, Funding acquisition. **Nick S. Bennett:** Writing – review & editing, Supervision, Resources, Project administration, Funding acquisition.

**Declaration of competing interest**

The authors declared that they have no known competing financial interests or personal relationships that could have been perceived to affect the research presented in this paper.

**Data availability**

Data will be made available on request.

**Acknowledgement**

The SmartSat Cooperative Research Council and the University of Technology Sydney (UTS) jointly funded this study, with additional support provided by Romar Engineering Pty. Ltd. for the 3D printing of heat sinks. The UTS and high-performance computing facilities were utilized for experimental work and numerical modelling, respectively.

## References

- [1] S.M. Sohel Murshed, C.A. Nieto de Castro, A critical review of traditional and emerging techniques and fluids for electronics cooling, *Renew. Sust. Energy Rev.* 78 (2017 oct) 821–833.
- [2] Saad Mahmoud, Aaron Tang, Chin Toh, Raya AL-Dadah, Sein Leung Soo, Experimental investigation of inserts configurations and PCM type on the thermal performance of PCM based heat sinks, *Appl. Energy* 112 (2013 dec) 1349–1356.
- [3] Ronan Grimes, Ed Walsh, Pat Walsh, Active cooling of a mobile phone handset, *Appl. Therm. Eng.* 30 (16) (2010 nov) 2363–2369.
- [4] Kh. Hosseinzadeh, M.A. Erfani Moghaddam, A. Asadi, A.R. Mogharrebi, D.D. Ganji, Effect of internal fins along with hybrid nanoparticles on solid process in star shape triplex latent heat thermal energy storage system by numerical simulation, *Renew. Energy* 154 (2020 jul) 497–507.
- [5] Kh. Hosseinzadeh, M.A. Erfani Moghaddam, A. Asadi, A.R. Mogharrebi, B. Jafari, M.R. Hasani, D.D. Ganji, Effect of two different fins (longitudinal-tree like) and hybrid nano-particles (MoS<sub>2</sub>-TiO<sub>2</sub>) on solidification process in triplex latent heat thermal energy storage system, *Alex. Eng. J.* 60 (1) (2021 feb) 1967–1979.
- [6] Kh. Hosseinzadeh, Elham Montazer, Mohammad Behshad Shafii, A.R.D. Ganji, Solidification enhancement in triplex thermal energy storage system via triplets fins configuration and hybrid nanoparticles, *J. Energy Storage* 34 (2021 feb) 102177.
- [7] Adeel Arshad, Mark Jabbar, Yuying Yan, Thermal performance of PCM-based heat sink with partially filled copper oxide coated metal-foam for thermal management of microelectronics, in: 2020 19th IEEE Intersociety Conference on Thermal and Thermomechanical Phenomena in Electronic Systems (ITherm), IEEE, 2020 jul..
- [8] Qinlong Ren, Zexiao Wang, Z.G. Qu Jianjun Zhu, Pore-scale heat transfer of heat sink filled with stacked 2d metal fiber-PCM composite, *Int. J. Therm. Sci.* 161 (2021 mar) 106739.
- [9] Qinlong Ren, Zexiao Wang, J.F. Tao Lai, Z.G. Qu Zhang, Conjugate heat transfer in anisotropic woven metal fiber-phase change material composite, *Appl. Therm. Eng.* 189 (2021 may) 116618.
- [10] Qinlong Ren, Penghua Guo, Jianjun Zhu, Thermal management of electronic devices using pin-fin based cascade microencapsulated PCM/expanded graphite composite, *Int. J. Heat Mass Transf.* 149 (2020 mar) 119199.
- [11] Z.G. Qu, W.Q. Li, W.Q. Tao, Numerical model of the passive thermal management system for high-power lithium-ion battery by using porous metal foam saturated with phase change material, *Int. J. Hydrog. Energy* 39 (8) (2014 mar) 3904–3913.
- [12] R. Srikanth, C. Balaji, Experimental investigation on the heat transfer performance of a PCM based pin fin heat sink with discrete heating, *Int. J. Therm. Sci.* 111 (2017 jan) 188–203.
- [13] Santosh Kumar Sahoo, Mihir Kumar Das, Prasenjith Rath, Application of TCE-PCM based heat sinks for cooling of electronic components: a review, *renew. Sustain. Energy Rev.* 59 (2016 jun) 550–582.
- [14] Adeel Arshad, Mark Jabbar, Pouyan Talebizadeh Sardari, Muhammad Anser Bashir, Hamza Faraji, Yuying Yan, Transient simulation of finned heat sinks embedded with PCM for electronics cooling, *Therm. Sci. Eng. Progress* 18 (2020 aug) 100520.
- [15] Hassan Nazir, Mariah Batool, Francisco J. Bolivar Osorio, Marlory Isaza-Ruiz, Xinhai Xu, K. Vignarooban, Patrick Phelan, Arunachala M. Inamuddin, Kannan, Recent developments in phase change materials for energy storage applications: a review, *Int. J. Heat Mass Transf.* 129 (2019 feb) 491–523.
- [16] Nidal H. Abu-Hamdeh, Khaled A. Alnefaie, Assessment of thermal performance of PCM in latent heat storage system for different applications, *Sol. Energy* 177 (2019 jan) 317–323.
- [17] Jose Pereira da Cunha, Philip Eames, Thermal energy storage for low and medium temperature applications using phase change materials – a review, *Appl. Energy* 177 (2016 sep) 227–238.
- [18] Rajesh Akula, C. Balaji, Thermal performance of a phase change material-based heat sink subject to constant and power surge heat loads: a numerical study, *J. Therm. Sci. Eng. Appl.* 13 (3) (2020 sep).
- [19] Adeel Arshad, Hafiz Muhammad Ali, Wei-Mon Yan, Ahmed Kadhim Hussein, Majid Ahmadlouydarab, An experimental study of enhanced heat sinks for thermal management using n-eicosane as phase change material, *Appl. Therm. Eng.* 132 (2018 mar) 52–66.
- [20] F. Mehling Harald, Cabeza Luisa, Phase change materials and their basic properties, in: NATO Science Series, Springer, Netherlands, 2007, pp. 257–277.
- [21] Gu Zhaolin, Hongjuan Liu, Yun Li, Thermal energy recovery of air conditioning system—heat recovery system calculation and phase change materials development, *Appl. Therm. Eng.* 24 (17–18) (2004 dec) 2511–2526.
- [22] Theodore D. Swanson, Gajanana C. Birur, NASA thermal control technologies for robotic spacecraft, *Appl. Therm. Eng.* 23 (9) (2003 jun) 1055–1065.
- [23] Mahmud M. Alkilani, K. Sopian, M.A. Alghoul, M. Sohif, M.H. Ruslan, Review of solar air collectors with thermal storage units, *renew. Sustain. Energy Rev.* 15 (3) (2011 apr) 1476–1490.
- [24] T. Arunkumar, D. Denkenberger, Amimul Ahsan, R. Jayaprakash, The augmentation of distillate yield by using concentrator coupled solar still with phase change material, *Desalination* 314 (2013 apr) 189–192.
- [25] Hafiz Muhammad Ali, Adeel Arshad, Experimental investigation of n-eicosane based circular pin-fin heat sinks for passive cooling of electronic devices, *Int. J. Heat Mass Transf.* 112 (2017 sep) 649–661.
- [26] Hafiz Muhammad Ali, Adeel Arshad, Muhammad Mansoor Janjua, Wajahat Baig, Uzair Sajjad, Thermal performance of LHSU for electronics under steady and transient operations modes, *Int. J. Heat Mass Transf.* 127 (2018 dec) 1223–1232.
- [27] X. Duan, G.F. Naterer, Heat transfer in phase change materials for thermal management of electric vehicle battery modules, *Int. J. Heat Mass Transf.* 53 (23–24) (2010 nov) 5176–5182.
- [28] A. Mahrous, Thermal performance of pcm based heat sinks, *Int. J. Mech. Eng.* 2 (4) (2013).
- [29] K.C. Nayak, S.K. Saha, K. Srinivasan, P. Dutta, A numerical model for heat sinks with phase change materials and thermal conductivity enhancers, *Int. J. Heat Mass Transf.* 49 (11–12) (2006 jun) 1833–1844.
- [30] Adeel Arshad, Hafiz Muhammad Ali, Shahab Khushnood, Mark Jabbar, Experimental investigation of PCM based round pin-fin heat sinks for thermal management of electronics: effect of pin-fin diameter, *Int. J. Heat Mass Transf.* 117 (2018 feb) 861–872.
- [31] Mustafa Yusuf Yazici, Mete Avci, Orhan Aydin, Combined effects of inclination angle and fin number on thermal performance of a PCM-based heat sink, *Appl. Therm. Eng.* 159 (2019 aug) 113956.
- [32] Jinlong Xie, Kok Fah Choo, Jianhua Xiang, Hsiao Mun Lee, Characterization of natural convection in a PCM-based heat sink with novel conductive structures, *Int. Commun. Heat Mass Transfer* 108 (2019 nov) 104306.
- [33] Muhammad Junaid Ashraf, Hafiz Muhammad Ali, Hazrat Usman, Adeel Arshad, Experimental passive electronics cooling: parametric investigation of pin-fin geometries and efficient phase change materials, *Int. J. Heat Mass Transf.* 115 (2017 dec) 251–263.
- [34] Rasool Kalbasi, Introducing a novel heat sink comprising PCM and air - adapted to electronic device thermal management, *Int. J. Heat Mass Transf.* 169 (2021 apr) 120914.
- [35] S.C. Fok, W. Shen, F.L. Tan, Cooling of portable hand-held electronic devices using phase change materials in finned heat sinks, *Int. J. Therm. Sci.* 49 (1) (2010 jan) 109–117.
- [36] Yi-Hsien Wang, Yue-Tzu Yang, Three-dimensional transient cooling simulations of a portable electronic device using PCM (phase change materials) in multi-fin heat sink, *Energy* 36 (8) (2011 aug) 5214–5224.
- [37] V. Shatikian, G. Ziskind, R. Letan, Numerical investigation of a PCM-based heat sink with internal fins, *Int. J. Heat Mass Transf.* 48 (17) (2005 aug) 3689–3706.
- [38] V. Shatikian, G. Ziskind, R. Letan, Numerical investigation of a PCM-based heat sink with internal fins: constant heat flux, *Int. J. Heat Mass Transf.* 51 (5–6) (2008 mar) 1488–1493.
- [39] R. Pakrouh, M.J. Hosseini, A.A. Ranjbar, R. Bahrampoury, A numerical method for PCM-based pin fin heat sinks optimization, *Energy Convers. Manag.* 103 (2015 oct) 542–552.
- [40] S.F. Hosseinzadeh, F.L. Tan, S.M. Moosania, Experimental and numerical studies on performance of PCM-based heat sink with different configurations of internal fins, *Appl. Therm. Eng.* 31 (17–18) (2011 dec) 3827–3838.
- [41] S.K. Saha, P. Dutta, Heat transfer correlations for PCM-based heat sinks with plate fins, *Appl. Therm. Eng.* 30 (16) (2010 nov) 2485–2491.
- [42] Huizhu Yang, Yongyao Li, Liang Zhang, Yonggang Zhu, Thermal performance enhancement of phase change material heat sinks for thermal management of electronic devices under constant and intermittent power loads, *Int. J. Heat Mass Transf.* 181 (2021 dec) 121899.
- [43] Amir Abdi, Viktoria Martin, Justin N.W. Chiu, Numerical investigation of melting in a cavity with vertically oriented fins, *Appl. Energy* 235 (2019) 1027–1040.
- [44] Rohit Kothari, et al., Analysis of solidification in a finite PCM storage with internal fins by employing heat balance integral method, *Int. J. Energy Res.* 43 (12) (2019) 6366–6388.
- [45] Rajesh Baby, Chakravarthy Balaji, Experimental investigations on thermal performance enhancement and effect of orientation on porous matrix filled PCM based heat sink, *International Communications in Heat and Mass Transfer* 46 (2013) 27–30.
- [46] Mohammad Ghalambaz, et al., Improving phase change heat transfer in an enclosure partially filled by uniform and anisotropic metal foam layers, *Int. J. Heat Mass Transf.* 228 (2024) 125678.
- [47] Hakim S. Sultan, et al., Improving phase change heat transfer in an enclosure filled by uniform and heterogenous metal foam layers: a neural network design approach, *J. Energy Storage* 85 (2024) 110954.